Available online at www.sciencedirect.com

SciVerse ScienceDirect

Ceramics International 39 (2013) 1087–1095

CERAMICS INTERNATIONAL

www.elsevier.com/locate/ceramint

Identification and quantification of reaction phases at Si_3N_4–Ti interfaces by using analytical transmission electron microscopy techniques

Orkun Tunckan[a], Hilmi Yurdakul[b], Servet Turan[b,*]

[a]School of Civil Aviation, Anadolu University, Iki Eylul Campus, TR-26480 Eskisehir, Turkey
[b]Department of Materials Science and Engineering, Anadolu University, Iki Eylul Campus, TR-26480 Eskisehir, Turkey

Received 20 April 2012; received in revised form 2 July 2012; accepted 6 July 2012
Available online 25 July 2012

Abstract

Silicon nitride (Si_3N_4) and titanium (Ti) were successfully bonded by using a capacitor discharge joining method. The resulting sample interfaces were characterized by scanning electron microscopy (SEM) and analytical transmission electron microscopy (TEM) techniques. SEM and chemical analyses by energy dispersive X-ray spectrometry (EDX) and wave length X-ray spectrometry (WDX) showed that if there is a reaction layer it is very small. Sample preparation from metal–ceramic joints for TEM by using conventional techniques is difficult. To overcome this problem, samples were prepared by using a focus ion beam (FIB) and investigated by TEM techniques. Analytical TEM techniques such as electron energy loss spectroscopy (EELS) revealed that Si_3N_4 interacted with Ti and reaction phases were formed at the interface. These phases are approximately 50 nm thick Ti_3N_2 layer at the interface next to Si_3N_4 followed by continuous Ti_6Si_3N phase as a matrix containing Ti_3N particles.

Keywords: Capacitor discharge joining; Electron microscopy; Si_3N_4; Ti

1. Introduction

Silicon nitride (Si_3N_4) based ceramics are used as turbochargers, valves, turbine components of engines and metal cutting tools in aerospace, automobile and electronic industries thanks to their excellent thermal resistance, oxidation resistance and high temperature mechanical properties [1–3]. However, Si_3N_4 is very difficult to machine due to its high hardness. Thus, joining is very important to produce complex shapes and to utilise their complementary properties with metals [4]. In practice, several methods for the joining have been developed in the last few decades, and different interlayer materials were used [5]. The most extensively used interlayer for Si_3N_4 based ceramics are Ag–Cu–Ti [6–8], Cu–Pd–Ti [9], Cu–Zn–Ti [10], Cu–Si–Al–Ti [11,12], Fe–Ni/Cu/Ni/Cu/Ni/Fe–Ni [13], stainless steel [14–16], super alloy [17], Mo [18], Ti/Ni multi interlayer [19], particulate added composite [20–23], Y_2O_3–Al_2O_3–SiO_2 [24] and oxide and oxynitride glasses [25].

Since the mechanical properties of joints are affected by the resulting interface characteristics, identification of new phase formations containing light elements like nitrogen (N) is necessary. Over the years, researchers have been investigating joint Si_3N_4–Ti (and/or Ti containing alloys) interfaces mostly by using SEM-EDX and X-ray diffraction (XRD) techniques [5–12,19–23,26–31]. By employing these techniques, the following phases were found at the interfaces: TiN and Ti_5Si_3 [6,8–12,21–23,26–32], Ti_2N [10], $TiSi_2$ [27], Ti_5Si_3, TiSi and TiN [26,30,31]. Based on the phase diagram of Ti–N [33,34], the formation of TiN, Ti_3N_2 and Ti_4N_3 [35], Ti_2N, Ti_3N and Ti_4N [36] phases are also possible. Interestingly, Ti_3N with a space group of P3 [37] and Ti_2N [38,39] formation were observed during plasma assisted nitridation of Ti–6Al–4V and surface nitriding of

*Corresponding author. Tel.: +90 222 321 35 50x6356; fax: +90 222 323 95 01.
E-mail address: sturan@anadolu.edu.tr (S. Turan).

0272-8842/$ - see front matter © 2012 Elsevier Ltd and Techna Group S.r.l. All rights reserved.
http://dx.doi.org/10.1016/j.ceramint.2012.07.031

Ti in arc plasma, respectively. However, SEM based chemical analysis techniques are not very reliable due to the bad spatial resolution resulting from the large electron beam broadening. In addition, considering XRD results do not yield the positions at which the phases were formed. In fact, there is no TEM work on Si_3N_4–Ti interfaces, but less amount of TEM work on Si_3N_4–Ti containing joint interfaces [6,7,9–12] since it is difficult to prepare a limited thin area at the desired interface to observe in TEM. In these TEM studies, traditional techniques such as bright field, dark field and diffraction techniques [6,7,9–12] were applied, but there is no quantification study of these reaction products with analytical TEM techniques.

Additionally, the joining process is generally time-consuming, and the reaction layers are thick. Therefore, the initial reaction mechanisms are not well understood. A recently developed capacitor discharge joining technique [28,40,41] provides an opportunity to study initial reactions since it is very fast and any resulting reaction layers are very thin. Therefore, the main purpose of this study is to prepare a thin TEM samples from the capacitor discharge joined Si_3N_4–Ti interfaces by using the focus ion beam technique and to quantify the reaction products formed at the initial stage of joining by using a reliable analytical TEM techniques such as electron energy loss spectroscopy analysis (EELS).

2. Materials and methods

2.1. Production of Si_3N_4–Ti joints

The materials used in this study were commercial Ti foil (99.9% pure, Goodfellow Ltd) and Si_3N_4 pieces (Ceramtec AG, Germany). The specimens to be joined were cut into 6 mm × 12 mm tiles and 4 mm thickness from the bulk materials using a diamond wafering saw. Afterwards, the joining surfaces of the tiles were polished starting with the 9 μm diamond suspension down to 20 nm colloidal silica surface finish by using automatic polishing machine (STRUERS). Prior to joining, the substrates and the foils were ultrasonically cleaned containing ethanol for 5 min. Finally, Si_3N_4 ceramics were joined by using the capacitor discharge joining technique with 10 μm thick Ti foil as an interlayer [28].

2.2. Sample preparation for SEM and TEM studies

After joining, joints were cut perpendicular to the width of each joint and the cutting samples were mounted in bakelite. Then, the mounted specimens for SEM investigations were prepared by polishing down to colloidal surface finish.

For thin TEM sample preparation, the focused ion beam (FIB)-SEM (FEI-Nova 600 NanoLab DualBeam™) technique was used by selecting a region from the interface of Si_3N_4–Ti joint on the SEM sample. Firstly, selected interface containing both Si_3N_4 and Ti was coated with a thin strip of protective platinum (Pt) layer. Then, surface was bombarded with gallium (Ga) ions from both sides of the protective layer. Since there is a difference in hardness and toughness between Si_3N_4 and Ti, the FIB parameters such as accelerating voltage and milling time must be carefully chosen. After, the sample was cut from the sides and bottom and lifted out by a microprobe then soldered to the TEM grid for final milling. After final milling, the specimen size was approximately 10 μm in length, 5 μm in width and less than 50 nm in thickness.

2.3. Microscopy studies

SEM samples were examined uncoated in a variable pressure field emission gun SEM (ZEISS Supra 50 VP) attached with an energy dispersive X-ray spectrometer (EDX-OXFORD Instruments) and wavelength dispersive X-ray spectrometer (WDX-OXFORD Instruments).

FIB prepared electron transparent samples were characterised by using 200 kV field emission gun (FEG)-TEM (Jeol 2100F) attached with high angle annular dark field scanning transmission electron microscope (STEM-HAADF) detector (Fishione), energy filter (Gatan GIF Tridiem) and parallel electron energy loss spectrometer (PEELS). In the STEM/EELS analysis, an electron spot with 1–2 nm in diameter was used and the acquisition time was chosen as 40 s live time. In STEM-EELS analysis, the convergence and collection semi-angles were 9.2 and 15.7 mrad, respectively. Furthermore, a drift corrector was used to avoid any possible drifts that may occur at nano-scale during acquisition of STEM-EELS analysis. The spectrometer energy dispersions were 0.2 and 0.5 eV/channels. The backgrounds of all acquired EEL and reference spectra were subtracted according to power-law in this study.

3. Results

3.1. SEM observations and WDX analysis

Considering the back scattered electron image (Fig. 1), Si_3N_4 was well bonded to Ti and cracks or voids were not observed along the interlayer and in the ceramic part. In addition, new phase formation was not detected at the interface. WDX line scan analyses were also carried out, and the results showed that high amount of N was detected across the interlayer (Fig. 1). However, this result was unacceptable because the interlayer should not have such a high amount of N as a result of the overlapping of $Ti_{L\alpha}$ and $N_{K\alpha}$. SEM-WDX line scan analysis also showed that Ti diffusion from the foil was not detected along the interface and the ceramic side. Although WDX is a very good technique to sort out overlapping problem, the spatial resolution of WDX is not better than EDX [40]. In conclusion, SEM-WDX and SEM-EDX techniques are not good enough to detect very small reaction layers and to quantify their compositions at the interfaces.

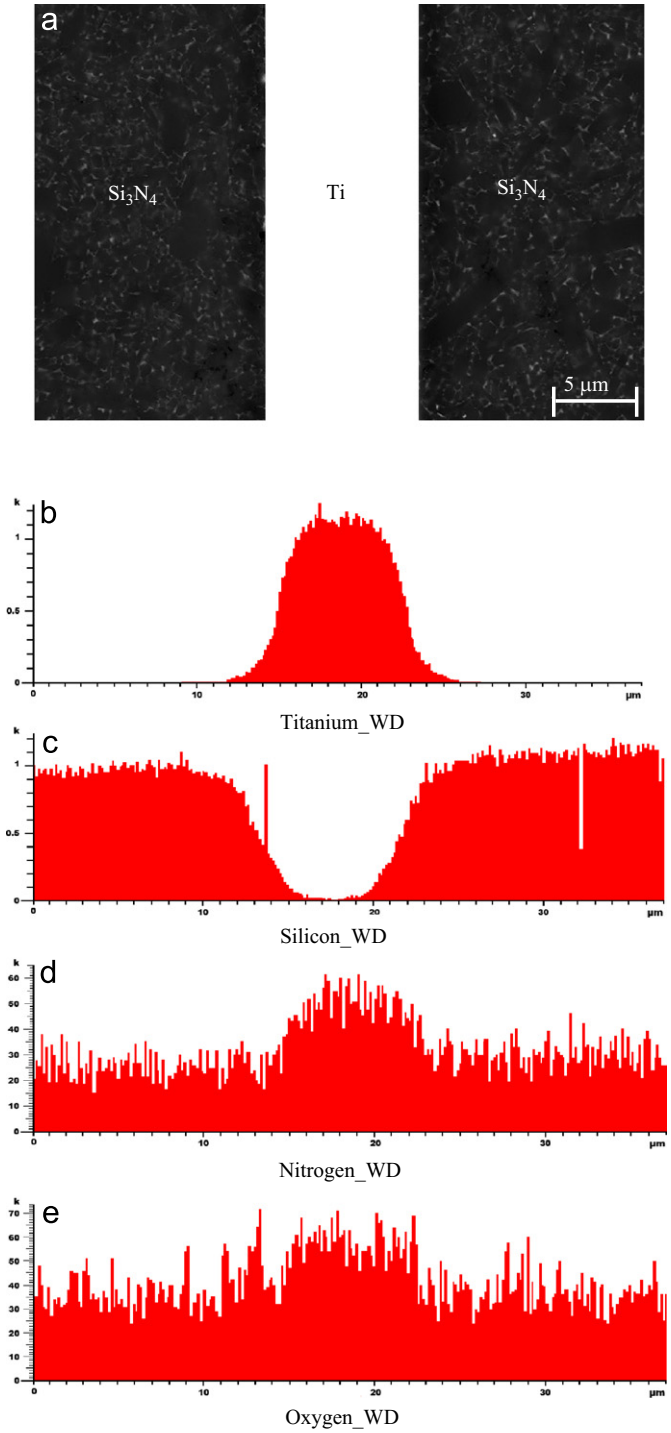

Fig. 1. (a) BEI image of Si_3N_4–Ti sample and WDX line scan analysis of Ti (b), Si (c), N (d) and O (e).

Techniques having a better spatial resolution together with quantification capabilities like TEM and EELS analyses must be used.

3.2. Analytical TEM observations

In order to clarify whether there is a reaction or diffusion at the Si_3N_4–Ti interface, TEM and STEM investigations were carried out (Figs. 2–8). Bright field TEM, STEM, STEM-HAADF and zero loss images of FIBed Si_3N_4–Ti joints are given in Fig. 2. According to these images, around 0.5 μm thick layer (RL) with a different microstructure was observed in comparison to the rest of the Ti interlayer. As can be clearly seen from the Z-contrast HAADF image in Fig. 2(d), some of the phases have white–grey contrast and dentritic forms, whereas STEM-BF image has contrary contrast for the same area (Fig. 2(c)). Thus, new phase formation in Ti interlayer was visually determined by a different contrast mechanism for different techniques. On the other hand, advantages of STEM techniques in comparison to TEM techniques were shown by these analyses since no different phase formation was observed by TEM-BF technique and elastic imaging. An indication of a reaction layer and an unsmooth interface can also be clearly seen between Si_3N_4 and Ti in a magnified image (Fig. 3).

In order to identify the chemical composition of these reaction products, EFTEM-3 window, EFTEM Spectrum Imaging (SI)-EELS and STEM-SI-EELS analyses were carried out (Figs. 4–8). These techniques are more suitable in comparison to TEM-EDX (performed but not given here) for chemical analysis in this system. Since Si_3N_4–Ti system includes a few elements and joining was performed in air, Si–$L_{2,3}$ (99 eV), N–K (401 eV), Ti–$L_{3,2}$ (456 eV) and O–K (532 eV) elements were chosen for EFTEM-3 window elemental mapping (Fig. 4(a–d)). According to EFTEM results, diffusion of Si and N to the Ti interlayer was determined. Similar to TEM and STEM (Fig. 2) images, spherical dark and light new phase formations are clearly seen in EFTEM-3 window elemental maps of the sample (Fig. 4(a–d)). Dendritic phase formation was also observed in Ti foil as shown in Fig. 4(a) and (b). From these maps, it was very difficult to conclude the presence of Si in these new phases; however, the chemistry of these phases can be formulated as Ti_xN_y. In order to reveal the chemical composition of these phases, quantitative EFTEM-3 window elemental mapping was performed (Figs. 5 and 6).

Fig. 5 shows quantitative EELS elemental mapping of N–K and Ti–$L_{3,2}$ edges obtained from EFTEM-SI (50–650 eV) analysis. The atomic quantities of Ti and N for point 1 (red) and point 2 (yellow) and Ti, N and Si for point 3 (white) were calculated from this image and shown in Fig. 5(b–h). According to Fig. 5(b,c) and (d,e), points 1 and 2 contained 59 at% Ti, 41 at% N and 76 at% Ti, 24 at% N, respectively. These results indicate that the reaction layer (point 1) has a composition of Ti_3N_2 whereas the spherically formed grains in Ti side (point 2) have a composition of Ti_3N. Also, atomic quantity of point 3 is calculated to be 59 at% Ti, 28 at% Si and 13 at% N (Fig. 5(f–h)) corresponding to $Ti_{0.59}Si_{0.28}N_{0.13}$ (approximately Ti_6Si_3N) which is very close to Ti_5Si_3N phase and similar to the expectations shown in a previous study [23]. Additionally, Ti is diffused from foil to the ceramic side through the grain boundaries (shown by red arrows in (Fig. 5(a)). In a

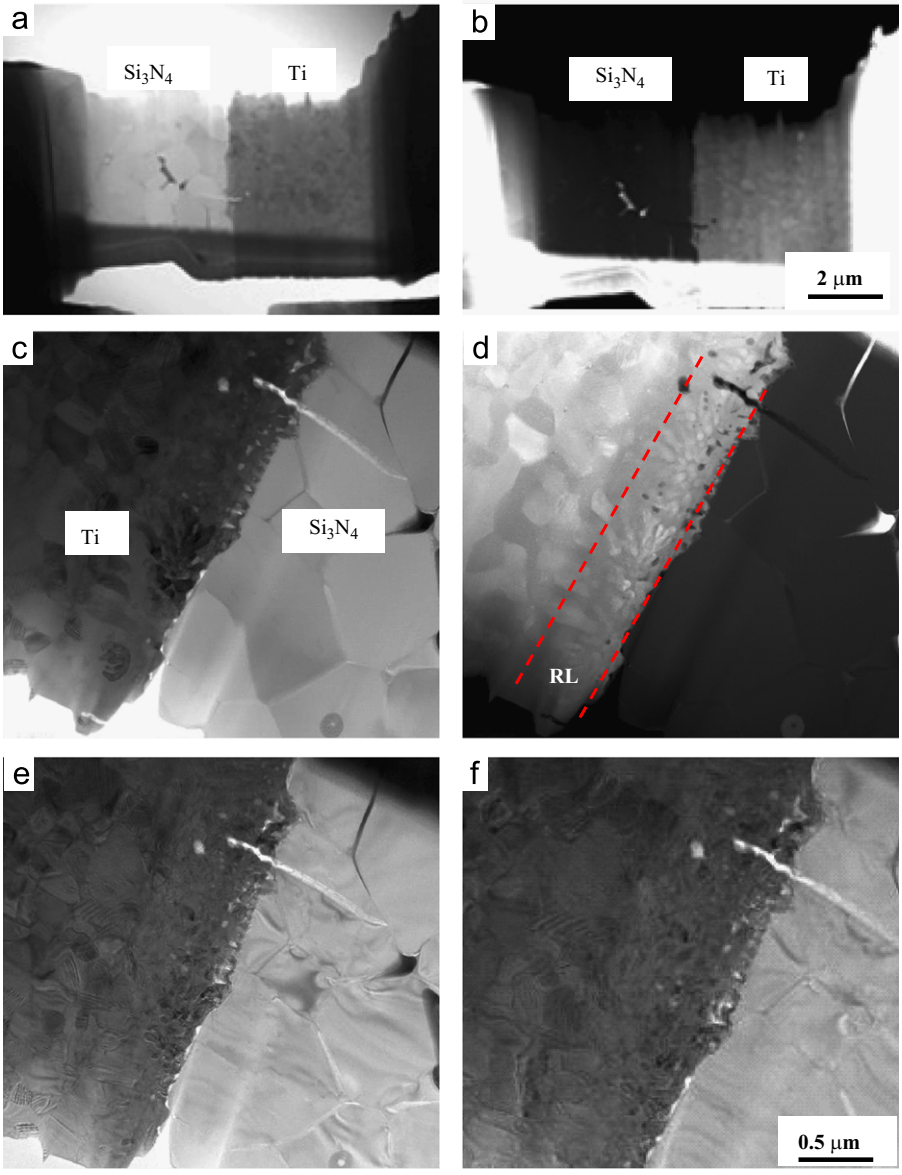

Fig. 2. (a) STEM-BF (b) STEM-HAADF (c) STEM-BF (d) STEM-HAADF (e) TEM-BF and (f) elastic images of FIBed Si_3N_4–Ti joints. RL: Reaction layer.

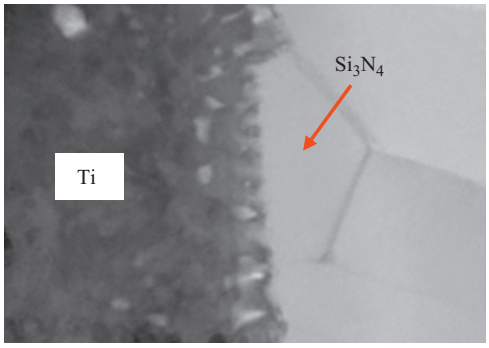

Fig. 3. Si_3N_4 and Ti interface in a magnified image showing unsmooth Si_3N_4 interface.

further line scan analysis (Fig. 6), it is shown that the formed phase is Ti_3N_2 by averaging the data along the red line between the points A and B.

In order to confirm the quantitative EFTEM-SI and EFTEM-SI-EELS analyses, STEM-SI-EELS analyses were also carried out (Figs. 7 and 8). Similar to previous analyses, Si and N reacted with Ti interlayer and formed spherical particles of Ti_xN_y in the Ti interlayer. In addition, surrounding phase of Ti_xN_y is found to be rich in Si and small amount of N was identified in the Ti foil corresponding to $Ti_xSi_yN_z$ phase (Fig. 7). Fig. 8 shows STEM-SI-EELS quantitative elemental maps obtained from STEM-SI analysis. The atomic quantity of Ti and N were calculated for different phases indicating that point 1 (yellow) is 62 at% Ti and 38 at% N (Fig. 8(b–c)) corresponding to the Ti_3N_2 phase and point 2 (red) is 76 at% Ti and 25 at% N (Fig. 8(d–e)) corresponding to the Ti_3N phase. With confidence, it can be stated that these results confirm the EFTEM-SI-EELS results. It should be noted that the $Ti_{0.59}Si_{0.28}N_{0.13}$ phase could not be

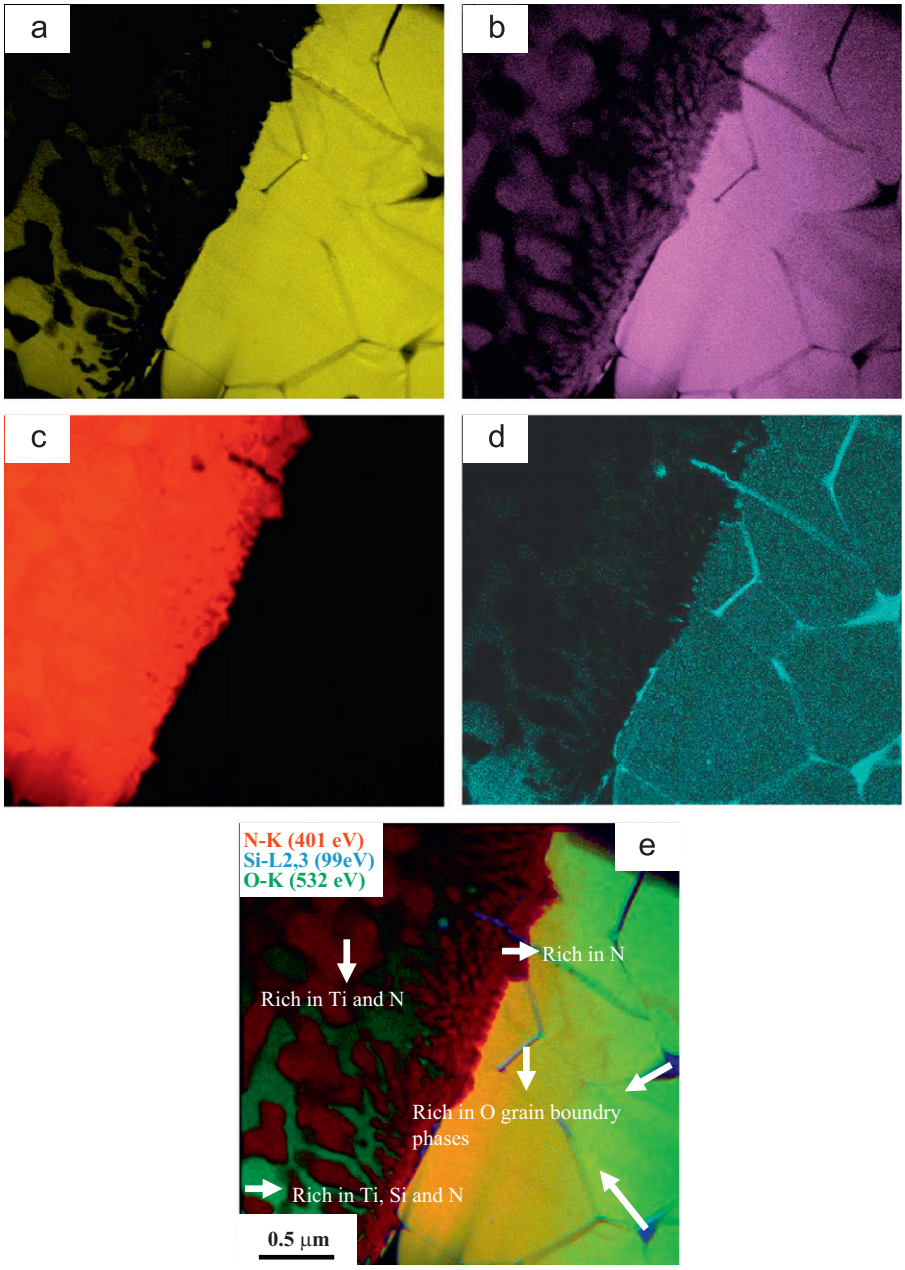

Fig. 4. (a) Si–$L_{2,3}$, (b) N–K, (c) Ti–$L_{2,3}$, (d) O–K edges and (e) RGB map of EFTEM-3 window elemental maps showing different phase occurrence at Si_3N_4–Ti interface.

quantified using the STEM-SI technique due to a high beam dose of a STEM probe in a low-loss electron energy region. From the results, the resulting microstructure after reactions is schematically drawn and shown in Fig. 9.

4. Discussion

When Si_3N_4 ceramics and Ti foils are joined, several chemical reactions occur between Si_3N_4 and Ti. Since Ti is a very strong nitride and silicate former, following reactions would take place:

$$Si_3N_4 + Ti = Ti_xN_y + Si_{(s)} \quad (1)$$

$$Si + Ti = Ti_xSi_y \quad (2)$$

$$Si_3N_4 + Ti = Ti_xSi_yN_z \quad (3)$$

In the literature, possibility of reaction 3 was presented without any thermodynamic data (34) whereas Gibbs free energies for the specific cases of reactions 1 and 2 (reactions 4–6) were given as below [11,12]:

$$Ti + 1/4Si_3N_4 = TiN + 3/4Si \quad \Delta G^o(J\ mol^{-1}) = -613000 + 40.8\ T \quad (4)$$

$$Ti + 2Si = TiSi_2 \quad \Delta G^o(J\ mol^{-1}) = -140200 + 5.44\ T \quad (5)$$

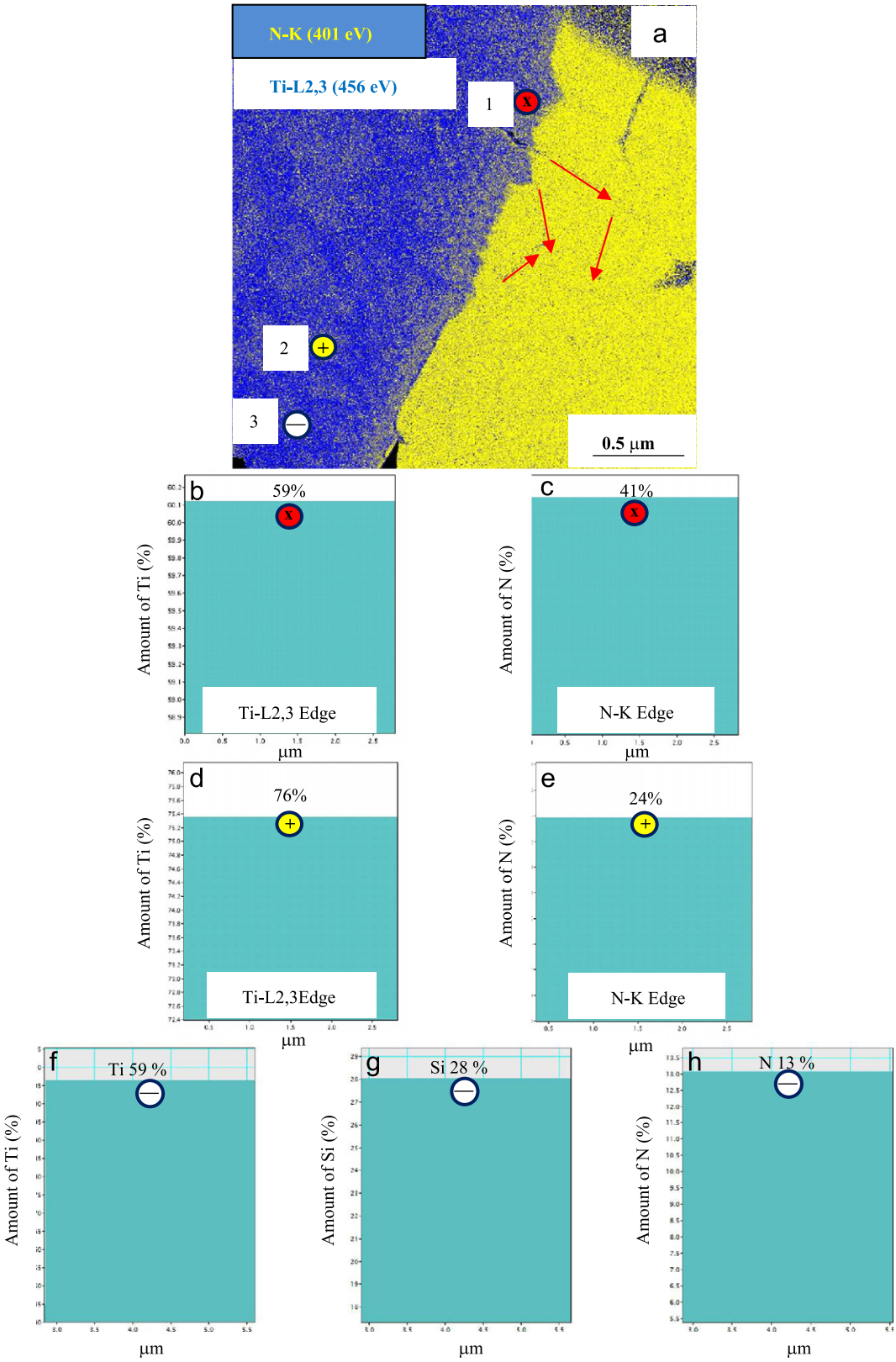

Fig. 5. (a) EFTEM-SI spectrum image (50–650 eV), (b,c) atomic quantity of Ti and N from the point 1 (marked with red), (d,e) atomic quantity of Ti and N from the point 2 (marked with yellow) and (f,g,h) and atomic quantity of Ti, Si and N from the point 3 (marked with white) in Fig. 5(a). (For interpretation of the references to color in this figure legend, the reader is referred to the web version of this article.)

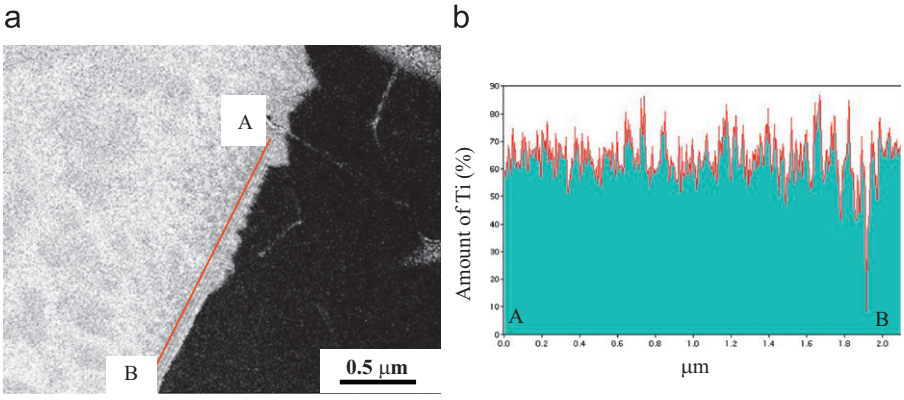

Fig. 6. (a) EFTEM-SI-EELS (Ti–L 456 ev) quantitative mapping for Si_3N_4–Ti sample (b) Ti/N relative composition given by quantitative line analysis along the red line between A and B. (For interpretation of the references to color in this figure legend, the reader is referred to the web version of this article.)

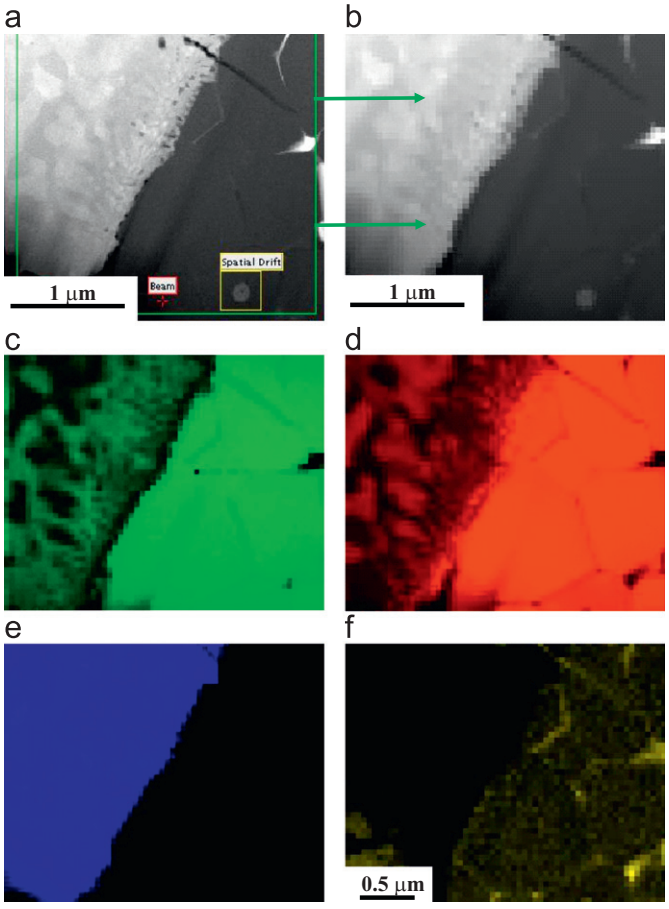

Fig. 7. (a) STEM-HAADF image showing where spectrum image area was acquired from (b) spectrum image and STEM-SI-EELS elemental mapping of (c) Si–$L_{2,3}$, (d) N–K, (e) Ti–$L_{3,2}$ and (f) O–K edges.

$$5Ti + 3Si = Ti_5Si_3 \quad \Delta G^{o}(J\ mol^{-1}) = -194140 + 16.74\ T \qquad (6)$$

According to TEM results obtained in this study, approximately 0.5 μm thick reaction zone formed at the interface consisting of 50 nm thick Ti_3N_2 reaction layer next to the

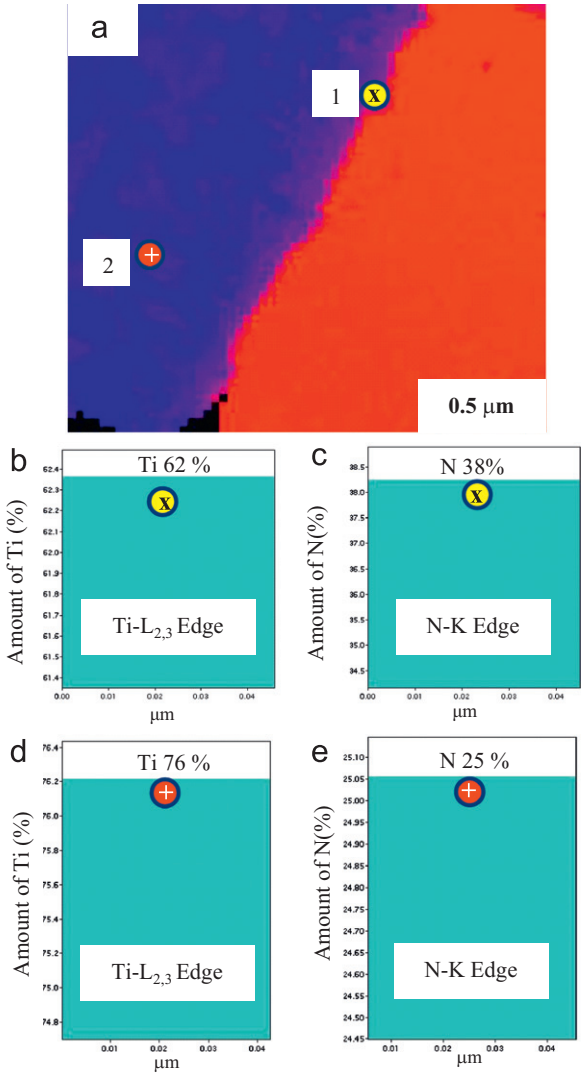

Fig. 8. (a) STEM-SI spectrum image, (b,c) atomic quantity of Ti and N from the point 1 (marked with yellow) and (d–e) atomic quantity of Ti and N from the point 2 (marked with red) in Fig. 8(a). (For interpretation of the references to color in this figure legend, the reader is referred to the web version of this article.)

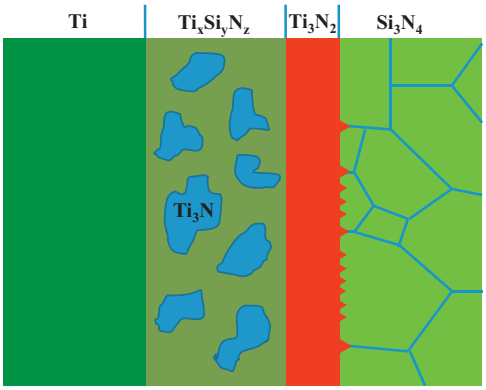

Fig. 9. Schematic view of microstructure at Si_3N_4–Ti interface.

Si_3N_4 followed by $Ti_{0.59}Si_{0.28}N_{0.13}$ (approximately Ti_6Si_3N) phase containing spherical Ti_3N grains. It is very important to state that these 3 phases were never observed at Si_3N_4–Ti interfaces. Although their formations were shown in the literature [35–39], no thermodynamical data for these reactions are available. Therefore, we propose the following reactions for the formation of these phases:

$$6Ti + Si_3N_4 \rightarrow 2Ti_3N_2 + 3Si \quad (7)$$

$$3Ti_3N_2 + 3Si \rightarrow Ti_6Si_3N + Ti_3N + 2N_{2(g)} \quad (8)$$

$$Ti_3N_2 \rightarrow Ti_3N + 1/2N_{2(g)} \quad (9)$$

$$3Ti_3N_2 + 3Ti \rightarrow 4Ti_3N + N_{2(g)} \quad (10)$$

$$2Ti_3N + 3Si \rightarrow Ti_6Si_3N + 1/2N_{2(g)} \quad (11)$$

From all the results and discussions, we believe that at the first stage, Ti diffuses to Si_3N_4 and react to form Ti_3N_2 reaction layer and free Si (reaction 7). Then, Ti_3N_2 and free Si further react to form Ti_6Si_3N and Ti_3N phases (reaction 8). Alternatively but less likely, Ti_3N phase may be formed by the dissociation of Ti_3N_2 phase (reaction 9) or reaction of Ti_3N_2 and Ti at the Ti side of the joint (reaction 10) and Ti_6Si_3N phase may be formed by the reaction between Ti_3N and Si (reaction 11).

5. Conclusion

Si_3N_4 and Ti joints were obtained by using a capacitor discharge joining technique enabling to study initial stage of reactions because of very rapid joining process. TEM samples from Si_3N_4–Ti interfaces were prepared by the using focus ion beam technique and investigated by using analytical TEM techniques. The results showed that a very thin reaction zone (0.5 μm) consisting of Ti_3N_2 layer next to Si_3N_4 interface followed by Ti_6Si_3N layer containing Ti_3N particles was formed. These are the first analytical TEM results through EFTEM, STEM and SI based EELS spectroscopy examines on the formation and identification of reaction phases at the Si_3N_4–Ti interface.

Acknowledgement

The authors wish to express their thanks to Anadolu University, Eskisehir, TURKEY for supporting this project under the BAP-030217 contract number. We also would like to thank Bilkent University UNAM laboratories for TEM sample preparation with FIB.

References

[1] L.M. Weldon, S. Hampshire, M.J. Pomeroy, Joining of ceramics using oxide and oxynitride glasses in the Y-SiAlON system, Journal of the European Ceramic Society 17 (1997) 1941–1947.
[2] F.L. Riley, Silicon nitride and related materials, Journal of the American Ceramic Society 83 (2000) 245–265.
[3] M.H. Bocanegra-Bernal, B. Matovic, Mechanical properties of silicon nitride-based ceramics and its use in structural applications at high temperatures, Materials Science and Engineering A 527 (2010) 1314–1338.
[4] M.M. Schwartz, in: M.M. Schwartz (Ed.), Joining of Structural Ceramics, Handbook of Structural Ceramics, 7, McGraw-Hill, USA, 1992, pp. 48–84.
[5] J.A. Fernie, R.A.L. Drew, K.M. Knowles, Joining of engineering ceramics, International Materials Reviews 54 (2009) 283–331.
[6] M. Nomura, C. Iwamoto, S.I. Tanaka, Nanostructure of wetting triple line in a Ag–Cu–Ti/Si_3N_4 reactive system, Acta Materialia 47 (1999) 407–413.
[7] D. Janickovic, P. Sebo, P. Duhaj, P. Svec, The rapidly quenched Ag–Cu–Ti ribbons for active joining of ceramics, Materials Science and Engineering A 304–306 (2001) 569–573.
[8] X.G. Song, J. Cao, Y.F. Wang, J.C. Feng, Effect of Si_3N_4 particles addition in Ag–Cu–Ti filler alloy on Si_3N_4/TiAl brazed joint, Materials Science and Engineering A 528 (2011) 5135–5140.
[9] J. Zhang, Y. Zhou, M. Naka, Interfacial microstructure of the Si_3N_4/Si_3N_4 joint brazed with Cu–Pd–Ti filler alloy, Journal of the European Ceramic Society | 26 (2006) 3459–3466.
[10] J. Zhang, C.F. Liu, M. Naka, Q.C. Meng, Y. Zhou, A TEM analysis of the Si_3N_4/Si_3N_4 joint brazed with a Cu–Zn–Ti filler metal, Journal of Materials Science 39 (2004) 4587–4591.
[11] M. Singh, R. Asthana, F.M. Varela, J.M. Fernandez, Microstructural and mechanical evaluation of a Cu-based active braze alloy to join silicon nitride ceramics, Journal of the European Ceramic Society | 31 (2011) 1309–1316.
[12] M. Singh, J.M. Fernandez, R. Asthana, J.R. Rico, Interfacial characterization of silicon nitride/silicon nitride joints brazed using Cu-base active metal interlayers, Ceramics International 38 (2012) 2793–2802.
[13] F. Fang, C. Zheng, H. Lou, R. Sui, Bonding of silicon nitride ceramics using Fe–Ni/Cu/Ni/Cu/Fe–Ni interlayers, Materials Letters 47 (2001) 178–181.
[14] A. Abed, P. bin Hussain, I.S. Jalham, A. Hendry, Joining of sialon ceramics by a stainless steel interlayer, Journal of the European Ceramic Society 21 (2001) 2803–2809.
[15] R. Polanco, A. Pablos De, P. Miranzo, M.I. Osendi, Metal–ceramic interfaces: joining silicon nitride–stainless steel, Applied Surface Science 238 (2004) 506–512.
[16] P. Poza, P. Miranzo, M.I. Osendi, Transmission electron microscopy study on silicon nitride/stainless steel bonded interfaces, Thin Solid Films 517 (2008) 779–781.
[17] J.J. Kim, J.W. Park, T.W. Eagar, Interfacial microstructure of partial transient liquid phase bonded Si_3N_4-to-Inconel 718 joints, Materials Science and Engineering A344 (2002) 240–244.
[18] A.E. Martinelli, R.A.L. Drew, Microstructure and mechanical strength of diffusion-bonded silicon nitride–molybdenum joints, Journal of the European Ceramic Society 19 (1999) 2173–2181.

[19] Z. Chen, M.S. Cao, Q.Z. Zhao, J.S. Zou, Interfacial microstructure and strength of partial transient liquid phase bonding of silicon nitride with Ti/Ni multi- interlayer, Materials Science and Engineering A 380 (2004) 394–401.
[20] G. Blugan, J. Kuebler, V. Bissig, J. Janczak-Rusch, Brazing of silicon nitride ceramic composite to steel using SiC-particle reinforced active brazing alloy, Ceramics International 33 (2007) 1033–1039.
[21] J. Zhang, Y.M. He, Y. Sun, C.F. Liu, Microstructure evolution of Si_3N_4/Si_3N_4 joint brazed with Ag−Cu−Ti+SiCp composite filler, Ceramics International 36 (2010) 1397–1404.
[22] Y.M. He, J. Zhang, Y. Sun, C.F. Liu, Microstructure and mechanical properties of the Si_3N_4/42CrMo steel joints brazed with Ag–Cu–Ti+Mo composite filler, Journal of the European Ceramic Society 30 (2010) 3245–3251.
[23] Y.M. He, J. Zhang, C.F. Liu, Y. Sun, Microstructure and mechanical properties of Si_3N_4/Si_3N_4 joint brazed with Ag−Cu−Ti+SiCp composite filler, Materials Science and Engineering A 527 (2010) 2819–2825.
[24] F. Zhou, Joining of silicon nitride ceramic composites with Y_2O_3–Al_2O_3–SiO_2 mixtures, Journal of Materials Processing Technology 127 (2002) 293–297.
[25] L.M. Weldon, S. Hampshire, M.J. Pomeroy, Joining of ceramics using oxide and oxynitride glasses in the Y-SiAlON system, Journal of the European Ceramic Society 17 (1997) 1941–1947.
[26] M.L. Santella, Brazing of titanium-vapor-coated silicon nitride, Advanced Ceramic Materials 3–5 (1988) 457–462.
[27] T. Shimoo, K. Okamura, S. Adachi, Interaction of Si_3N_4 with titanium at elevated temperatures, Journal of Materials Science 32 (1997) 3031–3036.
[28] S. Turan, D. Turan, I.A. Bucklow, E.R. Wallach, Microstructure of capacitor discharge joined SiAlON and silicon nitride ceramics, Institute of Physics Conference 168 (2001) 319–322.
[29] M. Maeda, R. Oomoto, T. Shibayanagi, M. Naka, Solid-state diffusion bonding of silicon nitride using titanium foils, Metallurgical and Materials Transactions 34 (2003) 1647–1656.
[30] J. Lemus, R.A.L. Drew, Joining of silicon nitride with a titanium foil interlayer, Materials Science and Engineering A352 (2003) 169–178.
[31] J.L. Ruiz, E.A. Aguilar-Reyes, Mechanical properties of silicon nitride joints using a Ti-foil interlayer, Materials Letters 58 (2004) 2340–2344.
[32] R.E. Loehman, Interfacial reactions in ceramic–metal systems, Ceramic Bulletin 68 (1989) 891–896.
[33] H.A. Wriedt, J.L. Murray, The N–Ti (Nitrogen–Titanium), Journal of Phase Equilibria 8 (1987) 378–388.
[34] H. Okamoto, N–Ti (Nitrogen–Titanium), Journal of Phase Equilibria 14 (1993) 536.
[35] W. Lengauer, The titanium–nitrogen system: a study of phase reactions in the subnitride region by means of diffusion couples, Acta Metallurgica et Materialia 39 (1991) 2985–2996.
[36] B. Holmberg, Structural studies on the titanium–nitrogen system, Acta Chemica Scandinavica 16 (1962) 1255–1261.
[37] J.C. Jiang, E.I. Meletis, TEM and simulation studies of Ti_3N ordered superstructure formed in intensified plasma assisted nitrided Ti–6Al–4V alloy, Thin Solid Films 402 (2002) 183–189.
[38] T. Bacci, L. Bertamini, F. Ferrari, F.P. Galliano, E. Galvanetto, Reactive plasma spraying of titanium in nitrogen containing plasma gas, Materials Science and Engineering: A 283 (2000) 189–195.
[39] S.C. Mishra, B.B. Nayak, B.C. Mohanty, B. Mills, Surface nitriding of titanium in arc plasma, Journal of Materials Processing Technology. 132 (2003) 143–148.
[40] S. Turan, I.A. Bucklow, E.R. Wallach, Capacitor-discharge joining of oxide ceramics, Journal of the American Ceramic Society 82 (1999) 1242–1248.
[41] K. Takaki, Y. Fujimaki, Y. Takada, M. Itagaki, T. Fujiwara, S. Ohshima, K. Oyama, I. Takahashi, T. Kuwashima, Bonding strength of alumina tiles joined using capacitor discharge technique, Surface and Coatings Technology 169–170 (2003) 495–498.